

Enantioselective Molecular Transport in Multilayer Graphene Nanopores

Youguo Yan,^{†,‡,⊥} Wen Li,^{†,‡,⊥} and Petr Král^{*,‡,§,||}

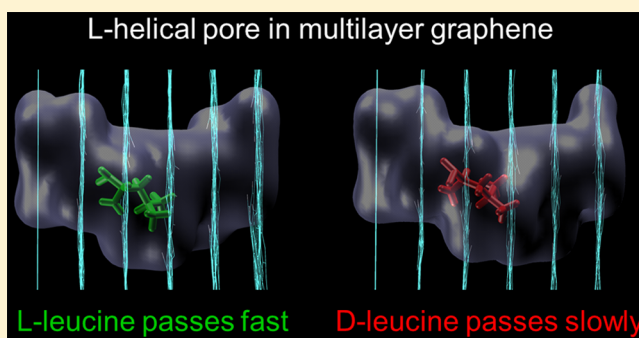
[†]College of Science, China University of Petroleum, Qingdao, Shandong, People's Republic of China, 102200

[‡]Department of Chemistry, [§]Physics, and ^{||}Biopharmaceutical Sciences, University of Illinois at Chicago, Chicago, Illinois 60607, United States

S Supporting Information

ABSTRACT: Multilayer superstructures based on stacked layered nanomaterials offer the possibility to design three-dimensional (3D) nanopores with highly specific properties analogous to protein channels. In a layer-by-layer design and stacking, analogous to molecular printing, superstructures with lock-and-key molecular nesting and transport characteristics could be prepared. To examine this possibility, we use molecular dynamics simulations to study electric field-driven transport of ions through stacked porous graphene flakes. First, highly selective, tunable, and correlated passage rates of monovalent atomic ions through these superstructures are observed in dependence on the ion type, nanopore type, and relative position and dynamics of neighboring porous flakes. Next, enantioselective molecular transport of ionized L- and D-leucine is observed in graphene stacks with helical nanopores. The outlined approach provides a general scheme for synthesis of functional 3D superstructures.

KEYWORDS: Molecular transport, multilayer graphene nanopores, enantioselectivity, molecular dynamics simulations



Soon after the discovery of carbon nanotubes,¹ it was hypothesized that these unique hollow nanostructures could support molecular transport in analogy to protein channels.² Eventually, a new area of nanofluidics was developed^{3–5} where many effects have been theoretically predicted and experimentally observed,^{6–12} such as various molecular drag phenomena.¹³

Once graphene sheets were isolated,^{14–17} they were also considered for nanofluidic applications. For example, liquids can fold graphene sheets into various nanostructures,¹⁸ including closed cells.^{19,20} Many opportunities in nanofluidics and related areas have emerged with the discovery of graphene nanopores.^{21–33} In analogy to protein channels, the selectivity of these quasi-2D pores is affected by chemical groups attached to the nanopore edges, having close contacts with the passing molecular species. Because of their large polarizability by the passing molecules, graphene nanopores provide a potential platform for molecular sensing, including DNA sequencing.^{34,35}

To bring the analogy with protein channels one step further, 3D nanopores could be designed from differently functionalized and stacked quasi-2D graphene nanopores. These nanopores could provide highly specific lock-and-key recognition by passing molecules with sequentially arranged nanopores edge groups, which might be exploited in highly selective molecular storage, removal, filtration and desalination.^{24,36–41} To pursue this idea, we use molecular dynamics (MD) simulations to

model molecular transport in such multilayer graphene nanopores.

Figure 1 shows model multilayer channels based on stacked hexagonal graphene flakes, with nanopores positioned close to their centers. In these flakes, H-terminated (anionic) and F–N-terminated (cationic) nanopores are used with (static) polarizations calculated while ions are present in their centers.²¹ The H-modified and F–N-modified pores have minimum pore diameters of 6.37 and 8.51 Å, respectively, to provide fast enough permeation of ions when prepared in stacked configurations (see Figure S1).

Once the hexagonal graphene flakes are assembled and released, individual flakes largely overlap with neighboring flakes, due to strong van der Waals (vdW) coupling.⁴² Therefore, nanopores formed within individual flakes become more or less aligned, depending on their separation from the flakes centers and mutual translations and rotations of neighboring flakes. Given their hexagonal symmetry, the neighboring flakes (separated by ≈ 3.35 Å) can be on average mutually rotated by 0° and $\pm 60^\circ$.⁴³ If the nanopores are asymmetrically positioned with respect to the flakes centers and the neighboring flakes are mutually rotated by the same angle (60°), where the rotation angle gradually increases with the

Received: July 5, 2017

Revised: September 29, 2017

Published: October 3, 2017

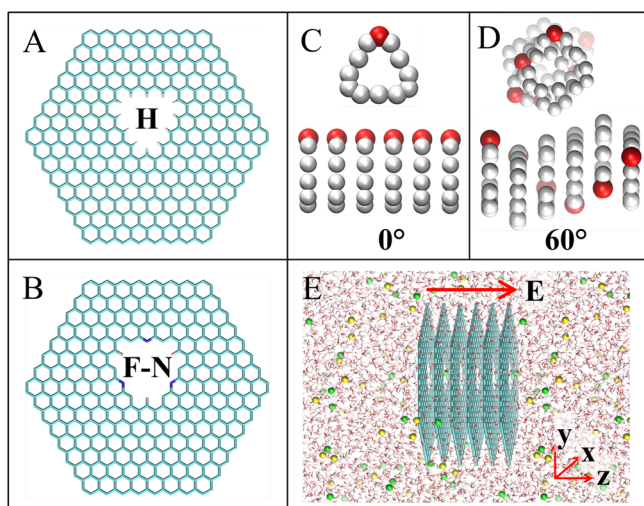


Figure 1. Hexagonal graphene flakes with H-modified (A) and F–N-modified (B) nanopores. The top- and side-views of typical H-modified channels of self-assembled graphene flakes with mutual rotation angles of 0° (C), 60° (D). (E) The self-assembled 0° channel in an ionic solution at the presence of an electric field.

flake number i ($i=60^\circ$), then the channels become chiral. In the simulations, all the flakes are either fixed (membranes), or they are free, except the leftmost graphene flake. At room temperature, the freely stacked flakes slightly vibrate and rotate around their equilibrium positions, which modulates the channels profiles.

The MD simulations were performed with NAMD,⁴⁴ using the CHARMM27 force fields⁴⁵ and the TIP3P water model.⁴⁶ Tables S1–3 show the atomic charges and Lennard-Jones (LJ) parameters used. The vdW coupling between different atomic groups was calculated with a cutoff distance of 12 Å, while the switching distance for nonbonded interactions was set to 8 Å. A particle mesh Ewald summation with periodic boundary conditions applied is used to describe the long-range Coulombic coupling.⁴⁷ The simulations were conducted in an NVT ensemble at $T = 298$ K with a time step of 1 fs where the temperature was controlled by the Langevin dynamics with a damping constant of $\gamma_{\text{Lang}} = 1 \text{ ps}^{-1}$.

In the first set of simulations, ionic solutions (NaF, NaCl, and NaBr in H-modified channel; LiCl, NaCl, and KCl in F–N-modified channel) with a concentration of 0.5 mol/L (in a box of $60 \times 60 \times 80 \text{ \AA}^3$) were driven through the above multilayer channels by an electric field of $E = 0.5 \text{ V/nm}$. Figure 2 shows the average ion flows through different 6-flake channels. The data were obtained from 105 ns simulations where the first 5 ns were used to stabilize the flow and the last 100 ns were used for analysis. The obtained results reveal that multilayer channels exhibit ion selectivity analogous to that seen in single-layer channels:²¹ (1) anions and cations can selectively pass through the H-modified and F–N-modified channels, respectively, and (2) larger ions have larger passing rates. However, multilayer channels also show new features: (3) fixed and freely moving channels have different transport regimes, where higher ion flows are in freely moving channels, and (4) channels with small rotation angles (larger pore overlaps) have larger ion flows.

The above (1,2) points could be explained in the same way like in the single-layer graphene nanopores,²¹ where the ion selectivity is caused by coupling of the passing ions to the

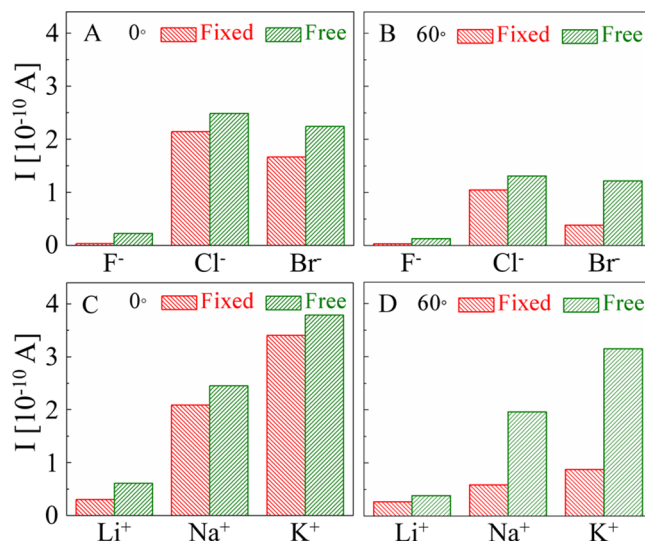


Figure 2. Ion flows through fixed and free channels at an electric field of 0.5 V/nm: (A,B) anionic H-channels with rotation angles of 0°, 60°, respectively; (C,D) same for cationic F–N-channels.

partially charged edge atoms of the nanopore rim. Larger ions can more easily shed their hydration shells and pass through the nanopores with higher rates. A comparison of ion flux between single-layer and multilayer ion channels indicates the multilayer channels possess higher ion selectivity, due to their elongated selection region (see Figure S2).

To understand the (3) point, notice that ions cannot easily adjust their hydration shells when passing through fixed multilayer channels. Therefore, it takes them longer to overcome larger barriers associated with this water rearrangement (see Figure S3). In contrast, hydrated ions can opportunistically sneak through freely moving multilayer channels, which results in their higher flows. This rearrangement of hydration waters is particularly difficult in rotated channels (60°), where individual nanopores are more mismatched (free flakes might fluctuate more), which explains the (4) point (see Movie S1 and S2). In twisted channels, as a consequence of a poor mismatch between adjacent flakes, the effective ion passage aperture is decreased and its transport path is increased, resulting in a smaller ion flow.

In Figure 3A,B, two distinct modes of ion transport through multilayer channels are observed (Movies S3 and S4). In channels with fixed flakes, ions tend to be trapped and later released by other passing ions. This ion passing dynamics can be called a “Coulomb knock-on” mode.^{48–53} In channels with freely moving flakes, individual ions mostly pass on their own (Figure 3B). In this “self-driven” mode, the vibrating flakes could dynamically trap and release the ions, which can pass relatively quickly through the entire channel (see Figure 3C and Figure S4). Ion trapping is partly caused by the fact that highly polarizable and spatially localized graphene flakes could act as local potential wells for the passing ions.^{5,48,54} This is amplified by the fact that in the current simulations, the flake polarization is considered to be static and calculated for an ion present in its pore, which means that all the flakes have always the same fixed partial charges favoring ion trapping.

In Figure 4, the potential of mean force (PMF) (free energy) for ions was calculated to probe physical forces governing ion transport through the channels. The PMF of a single ion along the channel axis (z -axis) was evaluated by an umbrella sampling

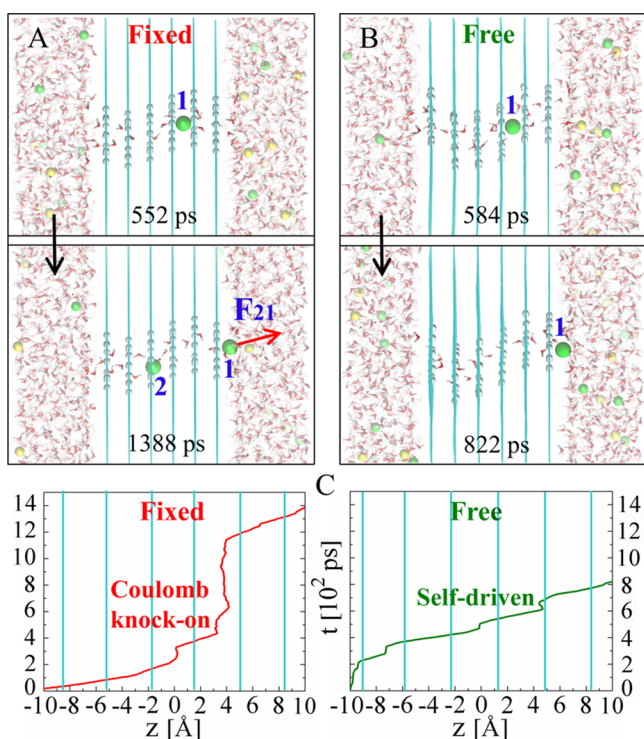


Figure 3. Two transport modes of Cl^- ions in H-channels with a rotation angle 60° . (A) A Coulomb knock-on transport mode seen in a fixed channel and (B) A self-driven transport mode seen in a free channel. (C) A typical time evolution curve of ion positions within the channels in the two transport modes; vertical lines denote the equilibrium positions of flakes.

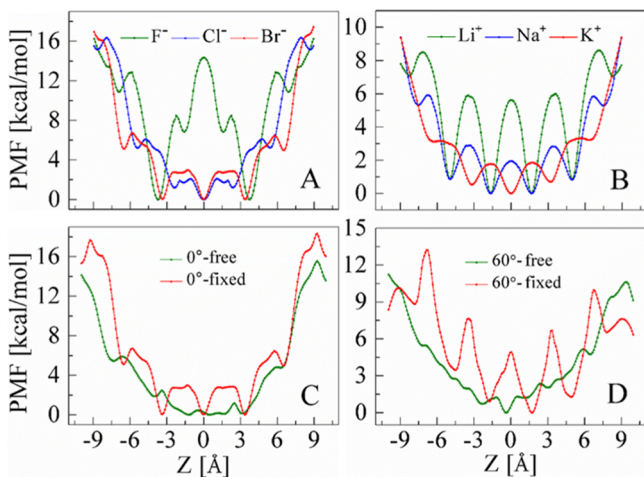


Figure 4. Potential of mean force profiles for ions passing through different channels: (A) anions in fixed H-modified 0° channels; (B) cations in fixed F–N-modified 0° channels; (C) Br^- in fixed and freely moving H-modified 0° channels; (D) Br^- in fixed and freely moving H-modified 60° channels.

method (see SI).^{55–57} The obtained energy barriers could be used to assess the blocking capability of channels for ion passage. Figure 4A clearly indicates that F^- must overcome high energy barriers, thus resulting in a low ion flux (Figure 2A). The PMF profiles also suggest that Cl^- could pass through the channel slightly easier than Br^- , thereby giving a slightly higher flux (Figure 2A). Similarly, the PMF profiles of cations (Figure 4B) match the fluxes observed in Figure 2B. Furthermore, using

Br^- as an example, we compared the PMF profiles of Br^- passing through fixed (free) 0° and 60° channels. The higher barriers present in the fixed systems (Figure 4C,D), especially at 60° , match the lower fluxes observed in those cases (Figure 2A,B). We also studied the dependence of ion flow on the channel length (number of flakes used) and electric fields (see Figures S5 and S6).

Electric field-driven flow of ions through these channels could also lead to electroosmosis.^{58–60} In Figure 5, we present

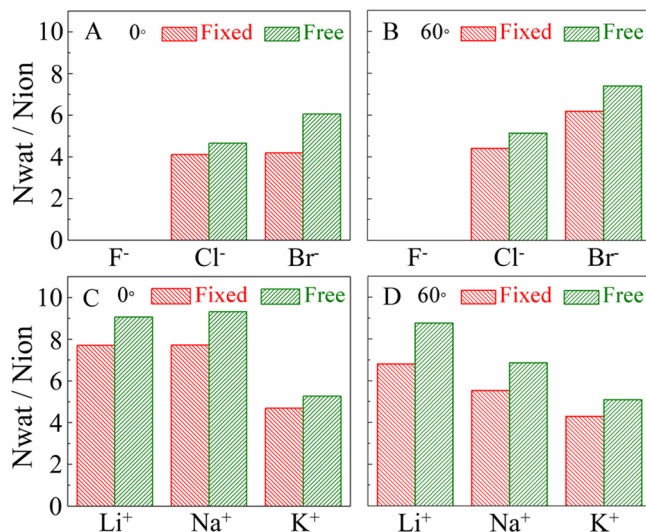


Figure 5. Rate of electroosmotic water flow in free and fixed multilayer channels: (A) H-channels with rotation angle of 0° ; (B) H-channels with rotation angle of 60° ; (C) F–N-channels with rotation angle of 0° ; (D) F–N-channels with rotation angle of 60° .

the average number of water molecules dragged by a single ion, given by the ratio $R = N_{\text{wat}}/N_{\text{ion}}$. The F^- data are omitted due to low values. For all the other ions, the electroosmotic drag is larger in free channels, since fixed channels can strip more water from the driven ions. Smaller anions with more hydrated waters drag less water through the H-channels, while smaller cations with more hydrated waters drag more water through the F–N-channels. This difference might be caused by a better stripping of anions in the ultranarrow H-channels than cations in the relatively wide F–N-channels.^{13,61} The effect of channel length on the electroosmosis is also examined (see Figure S7).

In recent years, enantioselective separation of chiral molecules became a viable possibility in synthetic nanopores.^{62–64} Therefore, in the second set of simulations, we investigated the transport of ionized L- and D-leucine molecules through H-modified free helical multilayer graphene channels (left helicity, $N = 6$) in an electric field of $E = 0.8 \text{ V/nm}$ (see Figure S8 in SI). Specially, we used local polarized graphene pores with simplified charge distributions because of the large leucine molecules (see details in SI). Figure 6 shows the number of leucine molecules passed through the channels in the last 150 ns of 200 ns long simulations. The passing rates are again higher for freely moving flakes and more overlapping channels. However, the enantioselectivity is observed only in the freely moving 60° (helical) channel (0° channel is not helical), where the L-leucine has twice larger transport rates than the D-leucine. The transport of L- and D-leucine molecules are mostly realized by the self-driven and Coulomb knock-on modes, respectively (see Movies S5 and S6). Note that in fixed

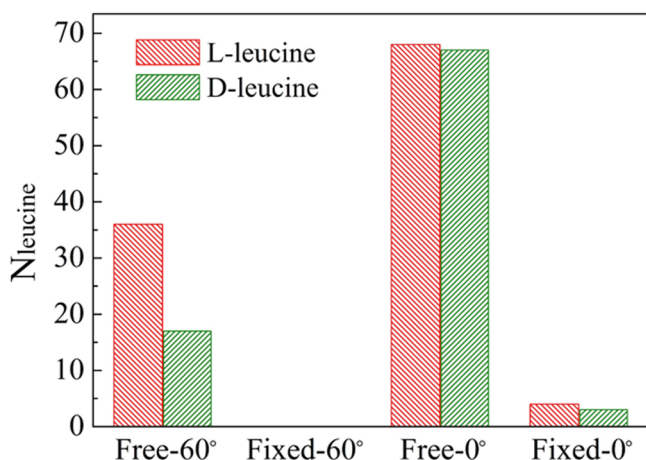


Figure 6. Number of passed L- and D-leucine molecules in H-modified channels with rotation angle of 0° and 60° at an electric field of 0.8 V/nm.

(0° and 60°) channels, the leucine molecules have very low passage rates (Figure 6), which indicates that a good enantioselectivity is only possible when the chiral molecules are tightly fitting the helical nanopores.

In summary, using MD simulations, we have studied ion transport in nanochannels formed by stacked porous graphene flakes. The simulations have revealed higher ion passing rates for larger ions, more overlapping pores, freely moving flakes, and shorter nanochannels. Coulomb knock-on and self-driven ion transport modes were revealed to be active in these channels. Electroosmosis associated with the ion passage was also observed. Stacked porous graphene channels with helical profiles show enantioselective molecular transport. In the future, highly selective channels, nesting sites, nanoreactors, mixers, and other nanofluidic devices could be prepared based on carefully designed multilayer stacked nanopores.^{62,65–69}

■ ASSOCIATED CONTENT

■ Supporting Information

The Supporting Information is available free of charge on the ACS Publications website at DOI: 10.1021/acs.nanolett.7b02846.

Method for measuring the nanopore sizes, LJ and charge parameters, ion selectivity of monolayer and multilayer graphene nanopores, ion dehydration and ion passing time in the multilayer graphene nanopores, method for PMF calculation, dependence of ion flow on channel lengths and electric field intensities, effect of channel length on electroosmosis and simulation details for enantioselective molecular transport (PDF)

Time dynamics of freely moving channels with mutually rotated angle of 0° (AVI)

Time dynamics of freely moving channels with mutually rotated of angle 60° (AVI)

Time dynamics of ion passing through fixed channels with mutually rotated of angle 0° (AVI)

Time dynamics of ion passing through freely moving channels with mutually rotated of angle 60° (AVI)

Time dynamics of L-leucine passing through freely moving channels with mutually rotated of angle 60° (AVI)

Time dynamics of D-leucine passing through freely moving channels with mutually rotated of angle 60° (AVI)

■ AUTHOR INFORMATION

Corresponding Author

*E-mail: pkral@uic.edu. Phone: +1-(312)-996-6318.

ORCID

Wen Li: 0000-0002-5362-8147

Petr Král: 0000-0003-2992-9027

Author Contributions

[†]Y.Y. and W.L. contributed equally.

Notes

The authors declare no competing financial interest.

■ ACKNOWLEDGMENTS

The research was financially supported by National Basic Research Program of China (2015CB250904), National Natural Science Foundation of China (51302321), and Fundamental Research Funds for the Central Universities (15CX08003A, 14CX0222A, 15CX05049A). P.K. was supported by the NSF DMR-1506886 grant.

■ REFERENCES

- (1) Iijima, S.; Ichihashi, T. *Nature* **1993**, *363*, 603–605.
- (2) Král, P.; Tománek, D. *Phys. Rev. Lett.* **1999**, *82*, 5373–5376.
- (3) Hummer, G.; Rasaiah, J. C.; Noworyta, J. P. *Nature* **2001**, *414*, 188–190.
- (4) Stein, D.; Kruithof, M.; Dekker, C. *Phys. Rev. Lett.* **2004**, *93*, 035901.
- (5) Vlasiouk, I.; Siwy, Z. S. *Nano Lett.* **2007**, *7*, 552–556.
- (6) Roux, B.; Allen, T.; Bernche, S.; Im, W. Q. *Q. Rev. Biophys.* **1999**, *37*, 15–103.
- (7) Zuo, G. C.; Shen, R.; Ma, S. J.; Guo, W. L. *ACS Nano* **2010**, *4*, 205–210.
- (8) Falk, K.; Sedlmeier, F.; Joly, L.; Netz, R. R.; Bocquet, L. *Nano Lett.* **2010**, *10*, 4067–4073.
- (9) Cao, Z.; Peng, Y. X.; Yan, T. Y.; Li, S.; Li, A. L.; Voth, G. A. *J. Am. Chem. Soc.* **2010**, *132*, 11395–11397.
- (10) Majumder, M.; Chopra, N.; Hinds, B. J. *ACS Nano* **2011**, *5*, 3867–3877.
- (11) Geng, J.; Kim, K.; Zhang, J. F.; Escalada, A.; Tunuguntla, R.; et al. *Nature* **2014**, *514*, 612–615.
- (12) Cha, T. G.; Pan, J.; Chen, H. R.; Salgado, J.; Li, X.; et al. *Nat. Nanotechnol.* **2013**, *9*, 39–43.
- (13) Král, P.; Wang, B. *Chem. Rev.* **2013**, *113*, 3372–3390.
- (14) Novoselov, K. S.; Geim, A. K.; Morozov, S. V.; Jiang, D.; Zhang, Y.; Dubonos, S. V. *Science* **2004**, *306*, 666–669.
- (15) Park, S.; Ruoff, R. S. *Nat. Nanotechnol.* **2009**, *4*, 217–224.
- (16) Kim, K. S.; Zhao, Y.; Jang, H.; Lee, S. Y.; Kim, J. M.; et al. *Nature* **2009**, *457*, 706–710.
- (17) Li, X. S.; Cai, W. W.; An, J. H.; Kim, S.; Nah, J.; et al. *Science* **2009**, *324*, 1312–1314.
- (18) Patra, N.; Wang, B.; Král, P. *Nano Lett.* **2009**, *9*, 3766–3771.
- (19) Park, J.; Zheng, H. M.; Lee, W. C.; Geissler, P. L.; Rabani, E.; Alivisatos, A. P. *ACS Nano* **2012**, *6*, 2078–2085.
- (20) Chen, Q.; Smith, J. M.; Park, J.; Kim, K.; Ho, D.; Rasool, H. I.; Zettl, A.; Alivisatos, A. P. *Nano Lett.* **2013**, *13*, 4556–4561.
- (21) Sint, K.; Wang, B.; Král, P. *J. Am. Chem. Soc.* **2008**, *130*, 16448–16449.
- (22) Jiang, D. E.; Cooper, V. R.; Dai, S. *Nano Lett.* **2009**, *9*, 4019–4024.
- (23) Pumera, M. *Energy Environ. Sci.* **2011**, *4*, 668–674.
- (24) Cohen-Tanugi, D.; Grossman, J. C. *Nano Lett.* **2012**, *12*, 3602–3608.

- (25) Garaj, S.; Liu, S.; Golovchenko, J. A.; Branton, D. *Proc. Natl. Acad. Sci. U. S. A.* **2013**, *110*, 12192–12196.
- (26) He, Z. J.; Zhou, J.; Lu, X. H.; Corry, B. *ACS Nano* **2013**, *7*, 10148–10157.
- (27) Celebi, K.; Buchheim, J.; Wyss, R. M.; Droudian, A.; Gasser, P.; Shorubalko, I.; Kye, J. I.; Lee, C.; Park, H. G. *Science* **2014**, *344*, 289–293.
- (28) Jain, T.; Rasera, B. C.; Guerrero, R. J. S.; Boutilier, M. S. H.; O'Hern, S. C.; Idrobo, J. C.; Karnik, R. *Nat. Nanotechnol.* **2015**, *10*, 1053–1057.
- (29) Jain, T.; Rasera, B. C.; Guerrero, R. J. S.; Boutilier, M. S. H.; O'Hern, S. C.; Idrobo, J. C.; Karnik, R. *Nat. Nanotechnol.* **2015**, *10*, 1053–105.
- (30) Rollings, R. C.; Kuan, A. T.; Golovchenko, J. A. *Nat. Commun.* **2016**, *7*, 11408.
- (31) Sahu, S.; Di Ventra, M.; Zwolak, M. *Nano Lett.* **2017**, *17*, 4719–4724.
- (32) Wei, G. L.; Quan, X.; Chen, S.; Yu, H. T. *ACS Nano* **2017**, *11*, 1920–1926.
- (33) Kim, H. W.; Yoon, H. W.; Yoon, S. M.; Yoo, B. M.; Ahn, B. K.; et al. *Science* **2013**, *342*, 91–95.
- (34) Branton, D.; Deamer, D. W.; Marziali, A.; Bayley, H.; Benner, S. A.; Butler, T.; et al. *Nat. Biotechnol.* **2008**, *26*, 1146–1153.
- (35) Min, S. K.; Kim, W. Y.; Cho, Y.; Kim, K. S. *Nat. Nanotechnol.* **2011**, *6*, 162–165.
- (36) Tagliacucchi, M.; Szeleifer, I. *Mater. Today* **2015**, *18*, 131–142.
- (37) Jirage, K. B.; Hultheen, J. C.; Martin, C. R. *Science* **1997**, *278*, 655–668.
- (38) Tokarev, I.; Minko, S. *Adv. Mater.* **2010**, *22*, 3446–3462.
- (39) Surwade, S. P.; Smirnov, S. N.; Vlassioux, I. V.; Unocic, R. R.; Veith, G. M.; Dai, S.; Mahurin, S. M. *Nat. Nanotechnol.* **2015**, *10*, 459–464.
- (40) O'Hern, S. C.; Boutilier, M. S. H.; Idrobo, J. C.; Song, Y.; Kong, J.; et al. *Nano Lett.* **2014**, *14*, 1234–1241.
- (41) Titov, A. V.; Wang, B.; Sint, K.; Král, P. *J. Phys. Chem. B* **2010**, *114*, 1174–1179.
- (42) Xia, D.; Xue, Q. Z.; Xie, J.; Chen, H. J.; Lv, C.; Besenbacher, F.; Dong, M. D. *Small* **2010**, *6*, 2010–2019.
- (43) Cohen-Tanugi, D.; Lin, L. C.; Grossman, J. C. *Nano Lett.* **2016**, *16*, 1027–1030.
- (44) Phillips, J. C.; Braun, R.; Wang, W.; Gumbart, J.; Tajkhorshid, E.; Villa, E.; Chipot, C.; Skeel, R. D.; Kale, L.; Schulten, K. *J. Comput. Chem.* **2005**, *26*, 1781–1802.
- (45) MacKerell, A. D.; Bashford, D.; Bellott, M.; Dunbrack, R. L.; Evanseck, J. D.; et al. *J. Phys. Chem. B* **1998**, *102*, 3586–3616.
- (46) Jorgensen, W. L.; Chandrasekhar, J.; Madura, J. D.; Impey, R. W.; Klein, M. L. *J. Chem. Phys.* **1983**, *79*, 926–935.
- (47) Darden, T.; York, D.; Pedersen, L. *J. Chem. Phys.* **1993**, *98*, 10089–10092.
- (48) Siwy, Z.; Heins, E.; Harrell, C. C.; Kohli, P.; Martin, C. R. *J. Am. Chem. Soc.* **2004**, *126*, 10850–10851.
- (49) Kopfer, D. A.; Song, C.; Gruene, T.; Sheldrick, G. M.; Zachariae, U.; de Groot, B. L. *Science* **2014**, *346*, 352–355.
- (50) Hummer, G. *Science* **2014**, *346*, 303.
- (51) Feng, J. D.; Liu, K.; Graf, M.; Dumcenco, D.; Kis, A.; Di Ventra, M.; Radenovic, A. *Nat. Mater.* **2016**, *15*, 850–855.
- (52) Krems, M.; Di Ventra, M. *J. Phys.: Condens. Matter* **2013**, *25*, 065101.
- (53) Kaufman, I. K.; McClintock, P. V. E.; Eisenberg, R. S. *New J. Phys.* **2015**, *17*, 083021.
- (54) Schoch, R. B.; Han, J. Y.; Renaud, P. *Rev. Mod. Phys.* **2008**, *80*, 839–883.
- (55) Torrie, G. M.; Valleau, J. P. *J. Comput. Phys.* **1977**, *23*, 187–199.
- (56) Kumar, S.; Rosenberg, J. M.; Bouzida, D.; Swendsen, R. H.; Kollman, P. A. *J. Comput. Chem.* **1995**, *16*, 1339–1350.
- (57) Roux, B. *Comput. Phys. Commun.* **1995**, *91*, 275–282.
- (58) Vuković, L.; Vokac, E.; Král, P. *J. Phys. Chem. Lett.* **2014**, *5*, 2131–2137.
- (59) Yusko, E. C.; An, R.; Mayer, M. *ACS Nano* **2010**, *4*, 477–487.
- (60) Daiguji, H. *Chem. Soc. Rev.* **2010**, *39*, 901–911.
- (61) Wang, B.; Král, P. *Phys. Rev. Lett.* **2008**, *101*, 046103.
- (62) Lim, T. W.; Son, Y.; Jeong, Y. J.; Yang, D. Y.; Kong, H. J.; Lee, K. S.; Kim, D. P. *Nat. Mater.* **2014**, *13*, 954–960.
- (63) Hauser, A. W.; Mardirossian, N.; Panetier, J. A.; Head-Gordon, M.; Bell, A. T.; Schwerdtfeger, P. *Angew. Chem., Int. Ed.* **2014**, *53*, 9957–9960.
- (64) Xue, M.; Li, B.; Qiu, S.; Chen, B. *Mater. Today* **2016**, *19*, 503–515.
- (65) Madhavan, N.; Robert, E. C.; Gin, M. S. *Angew. Chem., Int. Ed.* **2005**, *44*, 7584–7587.
- (66) Gilles, A.; Barboiu, M. *J. Am. Chem. Soc.* **2016**, *138*, 426–432.
- (67) Li, B.; Nam, H.; Zhao, J.; Chang, J.; Lingappan, N.; Yao, F.; Lee, T. H.; Lee, Y. H. *Adv. Mater.* **2017**, *29*, 1605083.
- (68) Wang, S. H.; Fan, Y. N.; Teng, J.; Fan, Y. Z.; Jiang, J. J.; Wang, H. P.; Grutzmacher, H. J.; Wang, D. W.; Su, C. Y. *Small* **2016**, *12*, 5702–5709.
- (69) Harnett, C. K.; Templeton, J.; Dunphy-Guzman, K. A.; Senousy, Y. M.; Kanouff, M. P. *Lab Chip* **2008**, *8*, 565–572.